Theoretical Investigation of Nucleophilic Substitution Reaction of Phenyl Carbonyl Isothiocyanates with Pyridines in Gas and Polar Aprotic Solvent

Keshab Kumar Adhikary[a],*, Francis Verpoort[b,c], Philippe M. Heynderickx[a,d],*

[a] Center for Environmental and Energy Research (CEER) – Engineering of Materials via Catalysis and Characterization, Ghent University Global Campus, 119-5 Songdomunhwa-Ro, Yeonsu-Gu, Incheon, 406-840 South Korea

[b] Laboratory of Organometallics, Catalysis and Ordered Materials, State Key Laboratory of Advanced Technology for Materials Synthesis and Processing, Wuhan University of Technology, Wuhan 430070, P.R. China

[c] National Research Tomsk Polytechnic University, Lenin Avenue 30, 634050 Tomsk, Russian Federation

[d] Department of Green Chemistry and Technology, Faculty of Bioscience Engineering, Ghent University, Coupure Links 653, Ghent, B-9000, Belgium

* Corresponding authors: Keshab.Adhikary@Ghent.ac.kr, Philippe.Heynderickx@Ghent.ac.kr

1. Abstract

This study focuses on the mutual interaction of substituents in the nucleophile and substrate – cross interaction constant, ρ_{XY}, in the uncatalyzed aminolysis by substituting pyridine with phenyl carbonyl isothiocyanate. The mechanism was found to be a stepwise process with a rate-limiting breakdown of the –NCS leaving group. This stepwise reaction mechanism considers the Cross-Interaction Constant (CIC) with rate-limiting breakdown of tetrahedral intermediate in gas and solvent phases. The corresponding Hammett coefficients are related to the substituents associated with (1) the nucleophiles (X), ρ_X (−1.93 to −6.54 for the gas phase and 10.5 to 18.9 in

the solvent model), and with (2) the substituents associated with the phenyl ring of the substrate (Y), ρ_Y (0.41 – 3.48 for the gas phase and 1.83 ~ −10.70 for the solvent model). It also includes the Brönsted coefficient with X, β_X (0.11 – 1.52 for the gas phase and −2.57 – 3.96 for the solvent model), and CIC values, ρ_{XY} (0.69 for the gas phase and 0.87 for the solvent model). In this work, the NBO analysis, reaction potential, reaction electronic flux (REF), dual descriptor, and the structure-energy relationships were considered in interpreting the mechanistic criteria.

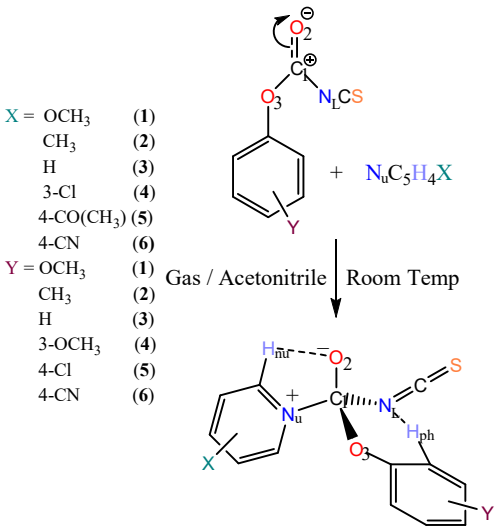

Scheme 1: Nucleophilic substitution reactions of aminolysis of Y-phenyl carbonyl isothiocyanates with X-pyridines in the gas phase and continuum acetonitrile solvent model.

Keywords: Cross-Interaction Constant (CIC), Pauling's empirical correlation (*s*), HOMO-LUMO interactions, Intrinsic reaction coordinate (IRC), Reaction electronic flux (REF), Dual Descriptors.

2. Introduction

Experimental information on nucleophilic substitution in carbonyl, sulphonyl and phosphoryl systems is abundantly available in the current literature survey. For example, Lee et al. [1–4] report a substantial contribution in the understanding of reactions of benzyl chlorides with phenoxides, while Tjuno [5], Castro [6,7] and Um [8,9] are worth noting with respect to their investigations on nucleophilic substitution reactions involving diethyl 4-nitrophenyl phosphate triesters.

By contrast, direct theoretical investigations of Hammett reaction parameters are rather scarce, often due to data inconsistencies. Therefore, this work intends to investigate the theoretical mechanistic criteria of organic nucleophilic substitution in carbonyl transfer reaction, using Hammett correlation, Brönsted substituent's effects [10,11], Cross-Interaction Constants (CIC) [12] and the reaction electronic flux[13–15] by analysis of data sets obtained from the high-level Gaussian calculations. This work specifically focuses on the aminolysis system, given in **Scheme 1**, where the nucleophilic substitution on >C=O is shown for different X and Y substituents. The effect of both substituents on the transition state(s) and possible intermediate(s) were investigated.

The CIC, ρ_{XY}, is defined in Eq. (1), where X and Y represent the substituent in the nucleophiles and/or Y in the substrates respectively. A Taylor series expansion[16] of log k_{XY} around $\sigma_X = \sigma_Y = 0$ (X = Y = H) leads to Eq. (2). Pure second, third or higher order derivative terms were not considered because they are normally too small[12]. The magnitude of ρ_{XY} is inversely proportional to the distance between X and Y through the reaction center.

$$\log \frac{k_{XY}}{k_{HH}} = \rho_X\sigma_X + \rho_Y\sigma_Y + \rho_{XY}\sigma_X\sigma_Y \quad (1)$$

$$\rho_{XY} = \frac{\partial^2 \log\left(\frac{k_{XY}}{k_{HH}}\right)}{\partial\sigma_X\partial\sigma_Y} = \frac{-\partial^2 \frac{(\Delta G^{\neq}_{XY} - \Delta G^{\neq}_{HH})}{2.303 \times RT}}{\partial\sigma_X\partial\sigma_Y} = \frac{\partial\rho_X}{\partial\sigma_Y} = \frac{\partial\rho_Y}{\partial\sigma_X} \quad (2)$$

In the stepwise process of the general substitution reaction, see **Scheme 2**, a mechanistic changeover can take place from rate-limiting breakdown, $k_N = K \cdot k_b = (k_a/k_{-a}) \cdot k_b$, to formation ($k_a$) of the intermediate (I) depending on (i) the relative basicity (pK_a) of the nucleophile (NX) and the nucleofuge (L/leaving group), and (ii) electron donating or electron withdrawing power of the non-leaving group (RY).

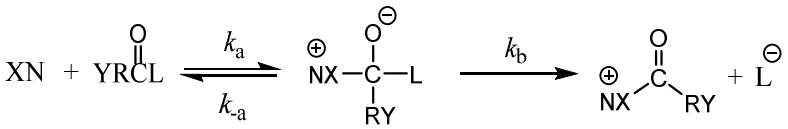

(3)

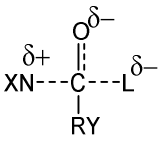

Intermediate (I)

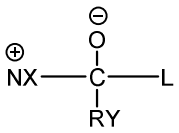

TS

Scheme 2: Pictorial representation of a nucleophilic substitution reaction.

If the involved nucleophile is strongly basic, it can be shown that, $k_{-a} << k_b$, so that $k_N = k_a$, whereas when the nucleophile is weakly basic, then $k_{-a} >> k_b$, and so $k_N = Kk_b$ and the latter term is the rate-determining step. Experimental results indicated that an electron donor Y ($\delta\sigma_Y < 0$) favors expulsion of the leaving group (or basic group), or conversely disfavors expulsion of the nucleophile (or weakly basic group) ($\delta\rho_X < 0$) in the stepwise mechanism with rate-limiting departure of the leaving group[17–19]. Thus $\rho_{XY} = \delta\rho_X/\delta\sigma_Y = (-)/(-) > 0$. On the other hand, weakly basic nucleophile ($\delta\sigma_X > 0$) was found to favor expulsion of the leaving group[17–21].

In the substitution reaction where the reactants are neutral, the constituted product is separated into two ions with opposite sign. Referring to **Scheme 2**, substitution regarding the aminolysis by substituted pyridines can be studied to analyze and estimate possible changes in transition state (TS) structures and the relative energies due to the effects of solvent, nucleophiles, and leaving

groups. Furthermore, it is crucial to note that the reactions were examined both in the gas phase and using a solvent model. The observations made during the initial steps of the reaction may be influenced by solvent polarization effects, which can impact the equilibrium state of the initialization process, as well as the intermediates and the transition state (TS) in **Scheme 2**. Characteristic observations along the reaction coordinate within the framework of the reaction force analysis are typically studied[13,22–24], and this helps to identify the chemical species that occur at different steps of the overall reaction. In order to rationalize the activation energy ($\Delta E^{\ddagger}$), we considered the Marcus equation[25] and the partition of $\Delta E^{\ddagger}$ provided by the reaction force analysis. For confirmation of the mechanistic criteria we analyzed the reaction electronic flux (REF)[13–15]. On the other hand, the TS with respect to reactants and products as well as reaction nature in terms of the Hammond postulate was quantified through the Brönsted coefficient[26] and the Marcus equation[25]. To identify the topological region of the molecular systems that are compatible with the electronic activity, we conducted the bond order as local descriptor[27] and the dual descriptor[28–30] that confirmed the REF results too.

While a chemical reaction proceeds, the reactant is transformed into product via a series of continuum structural changes, which can be seen in the IRC profile (E(ξ)), linking the TS to the reactants and products[31–35]. The reaction force[23,24,36] can be defined as d$E(\xi)$ with respect to reaction coordinate (IRC), see Eq. (4):

$$F(\xi) = -\frac{dE}{d\xi} \tag{4}$$

Stepwise processes are usually involved in four or more distinct regions along ξ. Through the value of ξ, the basic regions are the reactant (RC) region, the intermediate (I) region, the transition state (TS) region and product (PC) region. These reaction regions can be detected and

are helpful for locating and identifying the major reaction steps that provide an explanatory picture of the mechanism[22–24,37]. The reaction force scheme successfully speculates that the reaction works[36,38–41] generated by continuum decomposition of the activation and the reaction energies. Our process was distinctively isolated into six different steps, see Eqs. (5) and (6):

$$\Delta E^{\ddagger} = [E(\xi_{TS}) - E(\xi_{RC})] = W_1 + W_2 + W_3 + W_4 \quad (5)$$

$$\Delta E^{o} = [E(\xi_{PC}) - E(\xi_{RC})] = W_1 + W_2 + W_3 + W_4 + W_5 + W_6 \quad (6)$$

Where,

$$W_1 = -\int_{\xi_{RC}}^{\xi_1} F(\xi)d\xi > 0\,; \quad W_2 = -\int_{\xi_1}^{\xi_I} F(\xi)d\xi > 0; \quad W_3 = -\int_{\xi_I}^{\xi_2} F(\xi)d\xi > 0$$

$$W_4 = -\int_{\xi_2}^{\xi_{TS}} F(\xi)d\xi > 0; \quad W_5 = -\int_{\xi_{TS}}^{\xi_3} F(\xi)d\xi < 0; \quad W_6 = -\int_{\xi_3}^{\xi_{PC}} F(\xi)d\xi < 0 \quad (7)$$

All the reaction schemes are progressing through the IRC and within the regions where structural (W_1 and W_6) or electronic (W_2, W_3, W_4, and W_5) effects were implemented, see Eq. (7). These phenomena help to characterize the qualitative nature of the reaction and the activation energies. For insight into the nature of the TS, the $\Delta E^{\ddagger}$ can be rationalized in terms of the Marcus equation[25], see Eq. (8):

$$\Delta E^{\ddagger} = \triangle E_o^{\ddagger} + \frac{\triangle E^o}{2} + \frac{(\triangle E^o)^2}{16 \triangle E_o^{\ddagger}} \quad (8)$$

Here, $\triangle E_o^{\ddagger}$ represents the intrinsic activation energy and when $\triangle E_o^{\ddagger} = \triangle E^{\ddagger}$, then, $\Delta E^{o} = 0$.

Differentiation of the Marcus equation (8) leads to the Brönsted parameter[26], expressed in Eq. (9).

$$\beta = \frac{\partial \Delta E^{\ddagger}}{\partial \Delta E^{o}} = \frac{1}{2} + \frac{\Delta E^{o}}{8\Delta E_{o}^{\ddagger}} \quad (9)$$

Eq. (9) is related to the Leffler postulate[26], indicating the similarity of TS with respect to RC and PC. For the symmetric reaction β = ½ and for the asymmetric process either β > ½ or β < ½. Isoenergetic reactions present the TS at β =½, here the amount of activation work is equal to the amount of relaxation work. In contrast, exoenergetic reactions are characterized by an early TS if β < ½ and the amount of activation work is smaller than the relaxation work. On the other hand, an endoenergetic reaction is characterized through β > ½ and the amount of activation work is larger than the relaxation work. In this case, β can be considered as a descriptor of Hammond postulate[22,26] by giving qualitative information about the position and structure of the TS. Density functional theory (DFT)[42–48] provides information in terms of the response of the molecular system toward the variation of total number of electrons (N) and external potential, v(r). The change in N during the constant v(r) is the measure of the variation of electronic chemical potential (μ)[48] as in Eq. (10). This quantity is conceptually related to the electronegativity χ of a system[48]:

$$\mu = \left(\frac{\partial E}{\partial N}\right)_{v(r)} = -\chi \quad (10)$$

Applying the finite difference approximation[48], the value for μ can be calculated using ionization potential (I) and electron affinity (A) as shown in Eq. (11). Using Koopman's theorem[48] I and A can be formulated in terms of the frontier molecular orbital energies, where $A \approx -\varepsilon_{\mathrm{LUMO}}$ and $I \approx -\varepsilon_{\mathrm{HOMO}}$ and approximated as:

$$\mu \cong -\left(\frac{I+A}{2}\right) \approx \left(\frac{\varepsilon_{HOMO}+\varepsilon_{LUMO}}{2}\right) \quad (11)$$

It is possible to get the chemical potential at each point along the IRC generating the electronic chemical potential profile $\mu(\xi)$ in Eq. (12). The reaction electronic flux (REF)[13,14,38] is an essential tool to understand the electronic activity during the chemical reaction. It is defined as the negative of the derivative of μ with respect to the reaction coordinate,

$$J(\xi) = -\left(\frac{d\mu}{d\xi}\right) \tag{12}$$

The REF is the global descriptor for the electronic activity. From the classical thermodynamic point of view, a positive value for $J(\xi)$ is associated with spontaneous electronic activity that is driven by the process of bond strengthening or formation, and negative values for $J(\xi)$ should be associated to a non-spontaneous bond weakening or breaking along the reaction coordinate. The major primary target of this specific system is to understand the reaction mechanism of the organic carbonyl system having an isothiocyanate ligand in the field of valued medicinal compound synthesis[49]. For example, gluconasturtiin as an isothiocyano containing phenethyl isothiocyanate (PEITC) is present in many cruciferous vegetables shows a remarkable anti-cancer effects. The compound PEITC is already under clinical trials for leukemia and lung cancer[50]. Allyl-isothiocyanate (AITC) is an organosulfur phytochemical having the same potential found in in common cruciferous genera such as mustard, wasabi, and cabbage. AITC is metabolized through the mercapturic acid pathway, its specific pharmacokinetics and the biological functions of metabolites are still undefined. It is necessary to examine the inhibitory effects of AITC metabolites on lipid accumulation in vitro including its pharmacokinetics, and tissue distribution of AITC metabolites in animals and human[51]. Also it is worthy to provide an intensive analysis of known targets and mechanisms along with an activity test of isothiocyanates as a future anti-cancer drug.

To design biologically active compounds with antibacterial, antifungal, antimalarial, antifouling, and antitumoral properties, or to create nitrogen-containing drugs with valuable organic heterocycles, it is essential to employ isocyanide and isothiocyanate functional groups, or even a metal coordinating warhead[52], as unconventional pharmacophores.

A comprehensive review of experimental efforts is essential to understand the importance of theoretical calculations, as presented in this work. This review covers our previously published research and a current comparison with contemporaneous findings[53–59]. The aim is to determine the overall results of the ongoing computational investigation. In this framework, we clearly explain the significance of various treatments such as Hammett's and Brönsted coefficients, cross-interaction constants, reaction enthalpies and entropies, and relevant activation energies. Moreover, we painstakingly contrast the data obtained from our present study to establish significant correlations (Table **ST1** in the Supplementary Information, SI).

In the current system, the isothiocyanate ($^{-}$NCS) leaving group is involved and it is experimentally known to be a weak or bad leaving group[60–64]. Ample experimental observations regarding correlation coefficients between substituent effect and energy profile have been quantitatively reported for various systems[10,11]. Therefore, a comparable system, having a carbonyl center (Y-substituted phenyl carbonyl isothiocyanate, [(Y-C_6H_4O)(C=O)NCS], Eq. (13)), is selected for systematic theoretical analysis and comparison with other studied or under investigated experimental or computational systems.

In this study, the nucleophiles and substrates denoted by the set (XY) of the numbers, as mentioned in **Scheme 1**, were placed with the substituents, X = 4-MeO(1), 4-Me(2), H(3), 3-Cl(4), 4-Ac(5) and 4-CN(6); Y = 4-MeO(1), 4-Me(2), H(3), 3-MeO(4), 4-Cl(5) and 4-CN(6). For example, 'tsfD45' refers to the transition state structure that is formed by the interaction between

4-chlorophenyl carbonyl isothiocyanate and 3-chloropyridine in gas phase (in the solvent model it would be 'tssfD45'; D represented the dispersion calculated files).

$$[(Y\text{-}C_6H_4O)(C{=}O)NCS] + X\text{-}C_5H_4N \rightarrow [(Y\text{-}C_6H_4O)(C{=}O)(X\text{-}C_5H_4N^{+})](^{-}NCS) \quad (13)$$

3. Methodology

Computational methods play a significant role in many disciplines of chemistry ranging from drug to materials design. Recently used quantum mechanical (QM) modeling of chemical systems have reduced cost of high-accuracy models. The sampling and accuracy tradeoff is provided modeling with molecular mechanics (MM) in a multiscale QM/MM or iterative approach[65]. There is a plethora of techniques having a complexity of computational procedures, but commonly they use methods with the requirement of formal description of a molecular structure[66]. The common approach can be the description of connectivity, types of atoms, or bonds, or even energy correlations. When these descriptions are available to the modern chemical information systems, they do not necessarily allow computational techniques to be directly applied to them. By categorizing the descriptors[67], it is possible to employ in differential ways of interests, mechanisms, paths that are designed for specific classes of molecular systems to be analyzed.

The widely studied nucleophilic substitution in carbonyl transfer reactions usually proceeds through concerted or stepwise pathways[1,54–56,68–81] and the leaving group's ability is an important factor in determining its mechanistic lineament.

In this work, optimized stationary points were characteristically confirmed as local minima and transition state structures by harmonic force constant analysis. Intrinsic reaction coordinate (IRC) calculations were performed to verify the transition state structures [33,82]. Gibbs free energies were

in all cases computed by adding to the single-point energies both zero-point vibrational energies at 298 K obtained at the level of theory employed in the geometry optimization.

Since a substantial number of heavy atoms (18–30)are involved in the reaction system, the DFT self-consistent field molecular orbital (SCF-MO) method, B3LYP [83] with 6-311+G(d,p) basis set [84] was applied with empirical dispersion correction using GD3BJ code.

Geometries and the thermodynamic parameters (ΔE, ΔH, ΔG, ΔS) for relevant stationary points of all the species on the potential energy curve (PEC), reactants (R), nucleophile-substrate reactant complex (RC), transition state (TS), product-ion dipole complex (PC) were fully optimized without applying any symmetry constraints. Enthalpies, entropies and free energy of reaction (Eq. (13)) (ΔE^0, ΔH^0, ΔS^0, ΔG^0) and activation parameters ($\Delta E^{\ddagger}$, $\Delta H^{\ddagger}$, $T\Delta S^{\ddagger}$, $\Delta G^{\ddagger}$) were calculated at 298 K.

Single point calculations of the geometries coming from the IRC were performed at the above mentioned theory and level to find the relevant molecular properties. The dual descriptor was calculated on the stationary points using cube files in MultiWfn program[85]. We used IRC profiles of irc33 and the ircs33 only for the gas and the solvent model respectively without substituents. Finally, frequency calculation, SCRF-CPCM models (for solvent system), thermal corrections and free energies of gas and solvent polarization were evaluated with the same procedure. The vibrational analysis confirmed that (1) all reactants and products have positive frequencies and that (2) the transition states are true first-order saddle points on the potential energy surface. Free energies were evaluated where the gas phase and solution phase calculations were carried out on optimized geometries in their respective phases in accordance with their original parameterization.

Respective additional data tables and the figures are available in the Supplementary Information (SI). Supplementary Information is prefixed by 'ST' for Tables and 'SF' for Figures.

4. Results and discussion

In our study, the reaction of substituted phenyl carbonyl isothiocyanate with substituted pyridines was studied in the gas phase and continuum polarization solvent (acetonitrile) model. Recalling **Scheme 2**, a zwitterionic tetrahedral intermediate (**$T^{\pm}$**, see **Sketch 1**) can be observed for the aminolysis reaction of substituted phenyl carbonyl isothiocyano systems with an initial attack by the pyridine nucleophile (Pydn) and the rate-limiting breakdown of the isothiocyanate ($^{-}$NCS) leaving-group at the carbonyl moiety.

To investigate the true nature of the presented aminolysis reaction with different substituents, see **Scheme 1**, we have determined physical and thermodynamic parameters measured from the optimized reaction complexes (RC), product complexes (PC), and transition states (TS) in the gas and the solvent model. We used several treatments to analyze obtained structural features and the energy relationships. More specifically, the following sections describe and discuss detailed analysis on the bond perturbation, Pauling's bond valence-bond length empirical correlation, the NBO charges, energy profiles, the Hammett equation and corresponding cross-interaction constants, the reaction force and energy profile, the reaction electronic flux and the dual descriptor.

4.1. Structures and the Charge Function

In the TS series, the relative bond length variations (Δd) for $C_1 - N_u$ (Δd_{C1-Nu}), $C_1{=}O_2$ ($\Delta d_{C=O}$), $C_1 - N_L$ (Δd_{C1-NL}), and $C_1 - O_3$ (Δd_{C1-O3}) are summarized in **Table ST2b** for Y-substituents' variation in the gas phase and in **Table ST3a** for X-substituents' variation in the continuum

solvent model. Since the intrinsic thermodynamic properties are directly related to the bond perturbations[86], the slope, sign, and magnitude indicate the efficacious group's (substituent) participation in the TS. In **Table ST2b**, all the bond perturbations, such as for $C_1 - N_u$, $C_1 - O_3$, $C_1 = O_2$, and $C_1 - N_L$ are nicely correlated ($r^2 = 0.95 - 0.97$) with the variation of phen-ring Y substituent constants ($\delta\sigma_Y$), means direct electronic transmissions are effective. The smaller magnitude of correlation values for $C_1 - O_3$ (0.009) and $C_1 = O_2$ (-0.003) indicate smaller effects or transmission balanced between phen-ring and the carbonyl moiety, and the balance resulted in the relative propagation of pydn-ring and electronic perturbation of the weak leaving group – NCS. On the other hand, the somewhat larger correlation for $C_1 - N_u$ (slope = −0.030, $r^2 = 0.945$) and $C_1 - N_L$ (slope = 0.055, $r^2 = 0.965$ respectively (**Tables ST2b, SF2**) indicates the direct electronic transmission towards reaction center C_1 (negative value) and withdrawal (positive value). Conversely, in the case of the Hammett substituent constants for the nucleophilic variation ($\delta\sigma_X < |0| < \delta\sigma_X$) in the gas phase, a positive magnitude of the slope (0.022) for $C_1 - N_u$ bond perturbation is observed. This indicates the gradual obstruction of mutual charge transmission to the TS by gradual weaker interaction with the reaction center with a fair correlation coefficient, $r^2 = 0.949$ (**Table ST2a, Figure SF1a**).

For $C_1 - O_3$, and $C_1 = O_2$ and $C_1 - N_L$, poor correlation coefficients with small values were obtained for the slopes (-0.009, $r^2 = 0.687$; 0.003, $r^2 = 0.738$; and -0.003, $r^2 = 0.015$, respectively) for nucleophilic variation in the gas phase. **Table ST2a** and **Figure SF1a** show the detrimental charge and inductive effect to the reaction moiety by the protection to cleavage of the $C_1 - N_L$ bond. Interestingly, the departure of the leaving group strongly depends on the nucleophilic parity and the phen-ring participations. Also, on the same reaction center, the phen-ring perturbation enhanced the $C_1 - N_L$ bond cleavage with the nucleophile's interaction at the

carbonyl moiety. Hence, it can be expected that the TS is positioned closer to the product on the reaction coordinate, giving the late TS with a product-like structure in the gas phase.

The nature of the changes is somewhat different in the solution model (**ST3a**, **SF3a**), producing a gradual longer $C_1 - N_L$ bond lengths in the TS from strongly basic to weakly basic nucleophiles. The slope regarding the Hammett substituent constant is large positive (0.053), which corresponds to a gradual enhancement of bond breaking. On the other hand, sizeable positive C_1 - N_u bond saturation values indicate spontaneous close interaction of nucleophiles. Similarly, a considerable negative value for the slope (-0.011, see **ST3a** and **b**) is obtained, applying a Brönsted acid-base coefficient of the substituents in pyridine nucleophiles, where reasonable correlation coefficients between 0.848 and 0.904 were obtained.

A striking observation is the inefficiency of the leaving group ($^-$NCS) in the gas phase unlikely to be the polarized solvent continuum model concerning the nucleophilic variation. The high positive slope (0.053, r^2=0.848) indicates a large extent of $C_1 - N_L$ bond cleavage in the solvent model concerning the weakly basic nucleophiles. $C_1 - O_3$ and $C_1 = O_2$ actively enhance the leaving group departure with corresponding slopes –0.019 and –0.008 with good correlation coefficients. Details can be found in the section Bond Perturbation (Δd) in SI.

We intended to find the valence length correlation using Pauling's bond valence-bond length empirical parameters [87] expressed in Eq. (14).

$$s = \exp\left(\frac{R_0 - R}{b}\right) \tag{14}$$

Interestingly, this Pauling's bond softness *s* is a good indicator for destabilizing or stabilizing the reaction center. In practice, experimental[88] values for *b* have been reported as 0.25 to 0.55 Å. Due to the limited results, this value is often assumed to be a universal constant of 0.37 Å.

The Pauling's bond valence-bond length, *s*, for a Y-substituent's variation (for electron donating substituents there is $0 \geq \delta\sigma_Y$, and for electron withdrawing substituents, there is $\delta\sigma_Y \geq 0$) for gas, and the solvent model shows a common observation for the nucleophilic substitution at the carbonyl moiety, where nucleophilic charge transmission pushes forward the departure of the leaving group.

In the case of gas-phase nucleophilic substituent's variation (**ST4** or **ST4a**) from stronger basic to weaker (with possible variations $0 \geq \delta\sigma_Y$ or $\delta\sigma_Y \geq 0$, as aforementioned), the bond softness for $C_1 - N_u$ is gradually increasing, but for $C_1 - N_L$, it increases for 4-MeO pyridine to 3-Cl ($\delta\sigma_X \geq 0$) and gradually decreases for 3-Cl pyridine to 4-CN pyridine, ($\delta\sigma_X \geq 0$). The 3-Cl pyridine acquired the maximum magnitude (1.037). This observation suggested that stronger nucleophiles interacted within the closest proximity in advance by forming a very tight TS. On the other hand, weaker nucleophiles produce a long-distance weaker interaction where $C_1 - N_L$ leaving group departure was restricted. At this specific point $C_1 - O_3$ and $C_1 = O_2$ moieties play a vital as well as surprising role in TS tightness by employing remarkable shunt effects through the C_1 reaction center during the stronger and weaker nucleophilic attack.

Conversely, in the solvent model for the nucleophilic (X) substitution variation from stronger to weaker nucleophiles, a TS instability is observed for the stronger nucleophiles by the shunt effect, whereas it is stabilized by the weaker ones (**Table ST6** or **ST6a**). This phenomenon influences the advanced nucleophilic attack with the formation of a very tight TS with the action of stronger nucleophiles. The structural features (see **Table ST5a** and **ST5b**) indicate that two cyclic structures (**Figure 1**) are present, having five- and six-centered H-bonds. The corresponding H-bonds were bounded in 2.765 Å or less. The observations indicate the electronic shunting effects between the carbonyl bond and the phen-ring environment. The

reflection indicates extra stability to the transitional moments during the weaker nucleophilic interaction in the solvent model. The reason is an advanced nucleophilic attack leaving an N^+ nucleophile residue behind as a tetrahedral zwitterion intermediate (**T**$^{\pm}$). In the solvent model, the behavior is reasonably different mainly due to the solvent polarization. Details of the Pauling's Bond Valence-Bond Length Empirical Correlation can be found in SI.

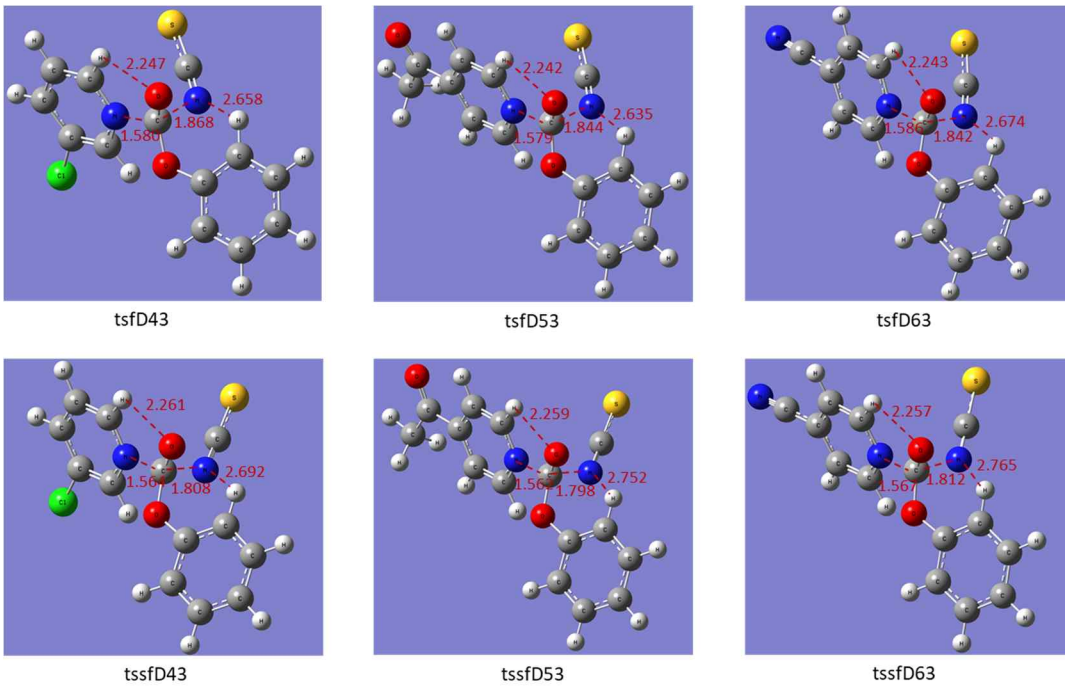

Figure 1. The TS structures of tsfD43, 53 and 63 of gas phase and the tssfD43, 53 and 63 of solvent model with relevant bond lengths (in Å) for comparison of the reaction moiety centered to C_1.

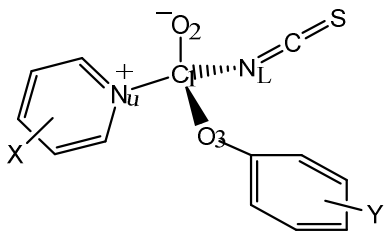

Sketch 1. Conceptual zwitterionic tetrahedral transition state structure ($T^{\pm}$).

A summary of the natural bond order charges (NBO charge), natural valence electron population (VPOP), Wiberg bond index (WBI), the bonding coefficients (BC), and the respective dipole moment (DM) of the TS in gas and solvent continuum models is displayed in **ST7a** and **b**. In the solvent model, the orbital population is gradually decreasing with the substituents' decreasing ability to donate. Leaving nitrogen (N_L) shows the increasing population with the variation of the nucleophilic substituents (X) from donating to withdrawing for the solvent model, whereas the population is similar for stronger to the weaker donor for the gas phase; i.e., consistent with the observation of bond softness. We can assume the pictorial representation of the charge density lobes in **Figure 2**.

NBO charges on carbonyl oxygen (O_2), nucleophilic nitrogen (N_u), and phen-ring oxygen (O_3), are indicating to the intersection route characteristics of the charge mobilization through the system's carbon reaction center (C_1). The EW nature of the Y-substituents affects the hybridization nature of the reaction center (C_1) in the solvent phase, tending to go from sp^2 to sp^3 by pushing ability by σ-inductive effects, resulting in a TS destabilization. On the other hand, the electronic charge on the leaving group's nitrogen (N_L) is mostly stable in the gas phase but is increasing in the solvent model. The positive charge accumulation in the C_1 reaction center and the negative charge centered on the N_L leaving nitrogen have a parallel nature where the strong donor and the weaker donor substituents play roles assertively, which is indicates the rate-

determining step change from formation to breakdown of the TS depending on the substituent's variation. Also in the gas phase, the charge flow towards the leaving group's nitrogen (N_L) is obstructed by creating a charge circulatory zone (shunt effect) between the reaction center, carbonyl group (C=O), and phen-ring. The positive charge in the C_1 reaction center and the negative charge accumulation in the leaving nitrogen N_L gradually increase with the substituents' gradual lower donating ability. The process reports the spontaneous charge separation by breaking the TS, probably due to the polarization function by ion-dipole interactions. This observation reflects in the dipole moment (DM) parameter in **Table ST7**, where the DM is higher in magnitude in the solvent model, and the gas phase is rather low and gradually decreases with the substituents' decreasing donor ability. That indicates charge delocalization takes place. However, the gas phase represents a competition of opening charge transformation through phen-ring to activate the departure of the leaving group depending on the substituents' variation. Details regarding the NBO charge can be found in SI.

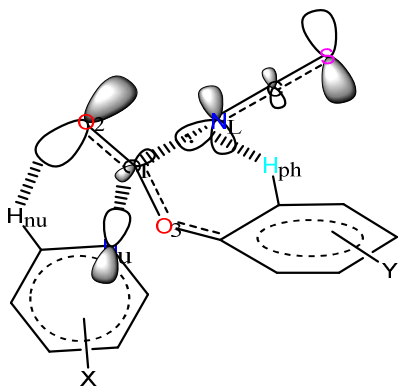

Figure 2. The schematic transition state diagram of the reaction between Y-phenoxy carbonyl isothiocyanates and X-pyridines.

4.2. Energy profile

This section reports the activation parameters, which were measured from the separated complex level. Due to space considerations, only selected results are presented here, while the full report can be found in the SI.

Examination of the shortened version of the results (**Table 1** and **Table ST8a** and **b**) reveals that the barrier heights, $\Delta G^{\ddagger}$, and the reaction energies, ΔG_o, of the pyridinolysis reaction, i.e., aminolysis by pyridines, are higher in the gas phase model, by ca. 23.0 ~ 5.0 and 27.0 ~ 6.0 kcal mol^{-1}, respectively, compared to the solvent model. These results can be attributed to the extreme destabilization of TS and formation of the PC by transforming the negative charge from carbonyl moiety to produce an ion-pair product. Also, two aromatic rings (pyridine and phenoxy) are expected to exert unfavorable effects due to steric crowding and electron donation. On the other hand, non-co-planar pyridine and phenyl rings impose H-bonded bound apparent ring structures: five-centered with the carbonyl oxygen and six-centered with the leaving nitrogen (N_L). This latter effect suggests that the TS is a rather tight and associative type with negative charge development on the C_1 reaction center in the gas phase. This assumption is consistent with observing the NBO charge on C_1 in the gas phase (vide infra ρ_Y>0; Section 4.3).

The entropy terms are practically similar, irrespective of the substituents X and Y (**Table 1**), and the magnitude differs little both in the gas (−1.0 ~ 3.0 cal mol^{-1}) and the solvent model (-2.0 ~ 2.0 cal mol^{-1}). The activation entropy differs a little: in the gas and the solvent phase, the magnitudes were -1.0 ~ 6.0 cal mol^{-1}. The trend of changes in $\Delta G^{\ddagger}$ and ΔG_o is quite similar in the gas phase. The weaker nucleophiles lead to higher values in both $\Delta G^{\ddagger}$ and ΔG_o, whereas the weakly basic phenyl ring in the system lowers the $\Delta G^{\ddagger}$ and ΔG_o. Since the reactions have high activation barrier and they are mostly endothermic in the gas phase model (and to a certain extent

in the solvent model) with highly structured TS (low entropies), experimental studies will not be suitable, especially in the case for the solvent phase.

In addition, solution phase reactions produced a higher degree of exothermicity for the electron-donating nucleophiles ($\delta\sigma_X \leq 0$) and electron-accepting Y-substituents ($\delta\sigma_Y \leq 0$). **Table 1** summarizes the activation enthalpies for the gas phase and the solution model. Strong electron-donating X and withdrawing Y is much more favorable for the early nucleophilic attack, governed by a value of 18.0 kcal mol^{-1} in the solution model. In contrast, weaker nucleophiles and strongly basic phen-ring compete with unfavorable by about 7.0 kcal mol^{-1}, where barrier height difference about 20.0 and 8.0 kcal mol^{-1} respectively for electron donor and withdrawing substituents in the gas and solvent model.

We conclude that the mechanism of the nucleophilic substitution reactions of Y-substituted phenyl carbonyl isothiocyanate is strongly dependent on the substituents (Y) in the substrate, the nucleophile, and the specific reaction medium.

4.3. The Hammett equation and CIC values

The Hammett equation[12] is a powerful tool for acquiring insights into reactivity theory. This tool expresses the relation between the reaction rate and the substituent constant in Eq. (1). The Hammett and Brönsted reaction constants, ρ_X, ρ_Y, β_X, and cross-interaction constants, ρ_{XY} (based on activation free energy, $\Delta G^{\ddagger}$, as in Eq. (2)) (ρ_X, ρ_Y, ρ_{XY}, and β_X are presented in bold) are collected for the gas and solvent model respectively in **Table 2** and **Table 3**. The Hammett (ρ_X) and Brönsted (β_X) coefficients with X and Hammett coefficients (ρ_Y) with Y in the gas and acetonitrile continuum model are displayed as having inadequate linear correlation coefficients. In **Table 2** and **Table 3**, the stronger π-acceptor substituent (X = 4-Ac and 4-CN) exhibits great positive deviations from the Hammett plots in the gas phase (**SF5a** and **SF6a** In contrast, the

relatively small deviation is exhibited in Brönsted plots (**SF5b** and **SF6b**) both in the gas and the solvent model. ρ_Y values are positive in the gas phase, whereas unusual $-\rho_Y$ values are observed in the solvent model. Usually, negative Hammett reaction constants ($\rho_Y<0$) are indicative of partial positive charge development at the adjacent atom of the reaction center[11]. Hence, in the present case, a positive charge develops in the O_3-atom of the phen-ring or a negative charge deployment from O_3 can be assumed.

The Hammett σ_p values of the π-acceptor substituents (4-Ac and 4-CN) represent the inductive and π-electron withdrawing effects. However, the experimental pK_a value only represents the inductive effect of X-substituted nucleophile because of the orthogonality of the σ-lone pairs and on the other hand separately exiting unaffected perpendicular ring π-system[11] remains. As a result, the protonation/deprotonation does not disturb the ring π-system[98–102]. Moreover, the positive charge center in the conjugate acid attracts π-electron inductively without π-conjugation between the σ-lone pair and the π-acceptor para substituent[11]. Hence, the pK_a values of π-acceptor substituents correctly reflect the substituent effects when the *N*-atom of pyridine becomes positively charged (azonium type, **Sketch 2**) in the TS.

Table 1. Enthalpies of reaction (ΔH_o), reaction energies (ΔG_o), activation enthalpies ($\Delta H^{\ddagger}$), activation energies ($\Delta G^{\ddagger}$) and the respective entropy changes ($-T\Delta S$) in the gas phase and in the solvent model (in brackets) are summarized.

System	$-T\Delta S_o$	$-T\Delta S^{\ddagger}$	ΔH_o	$\Delta H^{\ddagger}$	ΔG_o	$\Delta G^{\ddagger}$
13	-0.70 (-2.1)	-1.0 (-0.8)	12.5 (-11.5)	20.0 (1.1)	11.8 (-13.6)	19.0 (0.2)
23	1.5 (-0.9)	3.9 (0.4)	11.0 (-11.2)	17.7 (0.5)	12.5 (-12.0)	21.6 (0.9)
33	2.9 (-0.7)	3.0 (0.2)	13.0 (-10.0)	20.2 (0.9)	15.9 (-10.7)	23.3 (1.1)
43	3.1 (-0.9)	5.9 (2.7)	16.2 (6.7)	22.8 (16.3)	19.3 (5.8)	28.7 (19.0)
53	-0.3 (0.9)	1.4 (1.1)	14.1 (4.8)	21.8 (15.6)	13.8 (5.7)	23.2 (16.7)
63	2.4 (2.1)	5.1 (5.1)	15.9 (6.7)	24.4 (16.7)	18.3 (8.8)	29.5 (21.8)
31	0.6 (1.8)	3.1 (3.1)	12.1 (0.9)	19.6 (12.7)	12.7 (2.7)	22.7 (15.7)
32	3.5 (2.1)	3.6 (2.4)	12.8 (1.0)	20.4 (12.3)	16.2 (3.1)	24.1 (14.7)
33	2.9 (-0.7)	3.0 (0.2)	13.0 (-10.0)	20.2 (0.9)	15.9 (-10.7)	23.3 (1.1)
34	2.9 (2.4)	3.2 (6.2)	12.8 (1.4)	20.3 (11.7)	15.7 (3.7)	23.5 (17.9)
35	2.0 (-1.9)	4.6 (0.1)	13.0 (-8.4)	19.4 (1.4)	15.0 (-10.4)	24.0 (1.5)
36	2.9 (-0.9)	3.1 (2.6)	13.7 (-7.2)	19.4 (1.1)	16.6 (-8.1)	22.5 (3.7)

Table 2. Hammett and Brönsted coefficients and relevant cross-interaction constants (CIC) for the nucleophilic substitution reaction of Y-phenyl carbonyl isothiocyanates and X-pyridines in the gas phase.

X	σ_X[a]	ρ_Y	Y	σ_Y[a]	ρ_X	pK_a(X)[c]	β_X[b]
4-MeO	-0.27	**0.87**	4-MeO	-0.27	**-5.83**	6.47	**0.78**
4-Me	-0.17	**2.51**	4-Me	-0.17	**-4.78**	6.00	**1.06**
H	0	**0.41**	H	0	**-6.54**	5.17	**1.52**
3-Cl	0.37	**0.95**	3-MeO	0.12	**-1.93**	2.84	**0.11**
4-Ac	0.50	**3.48**	4-Cl	0.23	**-4.99**	3.51[d]	**1.13**
4-CN	0.66	**2.71**	4-CN	0.66	**-4.18**	1.90	**0.95**
ρ_{XY}[d]	**0.69 ± 0.3 (0.469)**						

[a] σ values were taken from reference [89]. [b] β_X values were determined using pK_a values in H_2O. The justification for this procedure is provided in references [3,90–94]. [c] pK_a values of pyridines in water at 25.0°C were taken from: [95–97]. [d] ρ_{XY} value was obtained using the multiple regression method followed by Eq. (1). The range of standard deviation for ρ_X, SD = 0.06 – 1.6, and r^2 = 0.034 – 0.914; For β_X, SD = 0.76 – 5.9 and r^2 = 0.003 – 880; For ρ_Y, SD = 0.08 – 3.50 and r^2 = 0.086 – 0.851.

Table 3. Hammett and Brönsted coefficients and relevant CIC for the nucleophilic substitution reaction of Y-phenyl carbonyl isothiocyanates and X-pyridines in acetonitrile solvent model.

X	σ_X[a]	ρ_Y	Y	σ_Y[a]	ρ_X	pK_a(X)[c]	β_X[b]
4-MeO	-0.27	**-1.75**	4-MeO	-0.27	**13.7**	6.47	**-2.88**
4-Me	-0.17	**1.83**	4-Me	-0.17	**14.1**	6.00	**-2.98**
H	0	**-9.30**	H	0	**18.9**	5.17	**-3.96**
3-Cl	0.37	**-1.58**	3-MeO	0.12	**14.1**	2.84	**-2.94**
4-Ac	0.50	**-10.7**	4-Cl	0.23	**17.3**	3.51[d]	**-3.70**
4-CN	0.66	**-1.42**	4-CN	0.66	**10.5**	1.90	**-2.57**
ρ_{XY}[d]	**0.87 ± 0.2 (0.752)**						

[a] σ values were taken from reference [89]. [b] β_X values were determined using pK_a values in H_2O. The justification for this procedure is provided in references [3,90–94]. [c] pK_a values of pyridines in water at 25.0°C were taken from: [95–97]. [d] ρ_{XY} value was obtained using multiple regression method followed by Eq. (1). The range of standard deviation for ρ_X, SD = 2.8 – 6.2, and r^2 = 0.502 – 0.921; For β_X, SD = 15.8 – 23.6 and r^2 = 0.682 – 0.942; For ρ_Y, SD = 0.04 – 13.9 and r^2 = 0.148 – 0.785.

In our work, large β_X values with an opposite sign for gas (+ve) and the solvent (-ve) model can be rationalized as we found remarkable sets of positive ρ_X and large negative β_X values for all the Y-substituents in the solvent model. Positive ρ_X and negative β_X indicate the more negative *N* atom in the nucleophile in the TS compared to its ground state. On the contrary, the gas phase showed a set of negative ρ_X with positive β_X values for all the Y-substituents. The magnitude of β_X values indicates the degree of electron transfer at the rate-determining step. The β_X values are in the range of 0.11 ~ 1.52 in the gas phase. This result is rationalized by forming $C_1 - N_u$ complete bonding for the stronger nucleophiles and partial for weaker ones. By contrast, the solvent model range of β_X values was -2.57 ~ -3.96. The unusually large positive ρ_X values (10.5 ~ 18.9) indicate the large degree of bond formation in the early stage of the TS.

The equilibrium rate value regarding the X-substituent, 3-Cl (4), and Y-substituent 3-MeO (4) is unusually large and deviated from the linearity in the normal Hammett plots. The overall rate equilibrium plots correlate better with the use of σ_p^+ or σ_p^- whereas the deviations remain at a certain level. As there is a positive and negative charge delocalization possible regarding the associated conjugate profile of the pyridine and phenyl rings in the tetrahedral intermediate or transitional point into the potential path, there are probably two distinct reasons behind the observation. In the TS (**Figure 2**), EW-nucleophile (3-Cl pyridine) generates a relatively stronger acidic proton adjacent to the nitrogen of the attacking nucleophile. On the other hand, EW phen-ring (Y = 3-MeO) failed to provide the localization of electron deficiency towards the ring-$C_1 - O_3$ moiety by applying resonance contributions. That stabilizes the carbocation reaction center for a relatively stronger nucleophilic attack enhanced by the H-bonding and extension of $n_\pi - p_\pi$ interaction. These are not equivalent to other *p*-substituted EW ligands. Contrary to the exhibited phenomena, in the solvent model, electron-withdrawing 4-Ac pyridine and 4-CN phen-ring

showed a minifying deviation in the rate equilibrium curve (**SF5a** and **6a**). The above observations are indicative of the dominating properties of certain substituent's effect of the nucleophile and substrate during the course of reaction. This effect works oppositely to destabilize the C_1 reaction center, and this results in a shift in equilibrium position. Determination of ρ_{XY} according to Eq. (1), giving the large positive magnitude of CIC: ρ_{XY} = 0.69 with the gas phase and ρ_{XY} = 0.87 with the solvent model. Based on this result, it is suggested that the reaction proceeds through a stepwise mechanistic path with a rate-limiting leaving group departure from the intermediate state. The large positive magnitude of ρ_{XY} implies that the nucleophile and the substrate are close enough to interact strongly. In other words, the degree of bond formation is really extensive in the TS for both gas and solvent phases. Although in the solvent phase, it is extraordinarily large with a larger ρ_{XY} value. This suggestion also agrees with the behavior of the strong π-acceptor para-substituent, X = 4-Ac in the X-pyridines in both phases.

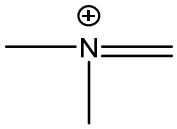

Sketch 2. Representation of the azonium ion.

4.6 Reaction force and energy profile

For the energy profile analysis, we have considered only the nucleophilic substitution (SN) process without the differential substitution interaction (XY=33) in the solvent and gas phase. Due to the advanced nucleophilic attack, the reaction profile is majorly controlled by the specific Y substituent. Generally, substituent effects can be expected to result in parallel reaction profiles, compared with the unsubstituted case (XY=33). Hence, by using the unsubstituted X and Y, it is possible to interpret the effect of various Y (and X) substituents.

We calculated the Intrinsic Reaction Coordinate (IRC), and all the steps were considered. **Figure 3** displays the energy profiles corresponding to the reaction in the gas and the solvent model. The reaction exhibits an endothermic behavior in the gas phase, but exothermic in the polar aprotic acetonitrile model. In the solvent model, the nucleophile and the substrate molecule initially form a high-energy adduct immediately after forming an active reaction complex (RC). The profile also indicates an existing tetrahedral intermediate in the reaction path.

The decreasing barrier height in the solvent model suggested that the relevant intermediate carries a substantial charge suitably stabilized by the solvent continuum polarization effects. This scenario also reflected the large positive ρ_X and negative β_X values (**Table 3**) during the Hammett and Brönsted substituents linear free energy correlation, where nucleophilic-*N* is expected to be more negative by incomplete charge transfer. The potential energy curve (**Figure 3**) reflects the active reaction zones throughout the gas and solvent model's intrinsic potential paths, where RC, I, TS, and the PC can be detected. We calculated the Brönsted coefficients (β) for the gas and solvent models. The β coefficient also notices properly about the Hammond postulate[103]. In the gas phase, we found a larger magnitude of $\beta = 0.54$, indicating a merely late product-like TS. In that consequence, $C_1 - N_L$ bond length in the products for gas and the solvent model for the system 43, 53 and 63 are 2.846 → 2.923, 2.850 → 2.924, and 2.900 → 2.926 Å, respectively. This indicates a good stabilization by solvation process and the corresponding TS are closer to the product state for the gas phase. In the solvent phase, $\beta = 0.13$ indicating a reactant-like transition state further indicating that the stabilization of the ion-pair produces a reactant-like TS. Note that the Marcus equation probably cannot be applied to the intermediate state, (I) because the reaction energy for the RC → I → ξ_2 is as large as the energy barrier ($\Delta E^{\neq} \sim \Delta E_o$) in the gas phase (24.90 kcal mol^{-1}). The intrinsic barrier hindering the reorganization of

leaving group departure and phenoxy non-leaving group reorganization, can be obtained from Eq. (8) with ΔE_o (for only TS, (I ~ ξ_3)) equals to -21.18 kcal mol^{-1} (**Table 4**). This gives an alternative intrinsic Marcus activation barrier of $\Delta E_o^{\neq}$ = 11.96 kcal mol^{-1}. According to the Marcus interpretation, Eq. (8) showed extremely higher order of structural reordering values in combination with the phenoxy non-leaving group reorganization compared to new $\Delta E^{\neq}$ = 3.71 kcal mol^{-1}. This means the remaining -8.25 kcal mol^{-1} might be associated with the electronic effects to form the ion-pair product complex. Using Eq. (9), TS analysis of the corresponding gas phase reactivity showed β = 0.59. This is in agreement with the Hammond postulate stating the endothermic reactions have a product-like transition state structure[104]. In contrast to the gas phase, the solvent model with exactly similar analysis flashes the β (**Table 4**) is rather remarkably smaller in magnitude (β = 0.13), indicating extremely early reactant-like TS, which is consistent with the previous observation of large negative Brönsted β_X values (**Table 3**). We also noticed the reaction force profile elsewhere and displayed this in **Figure 4** and **Table 4**.

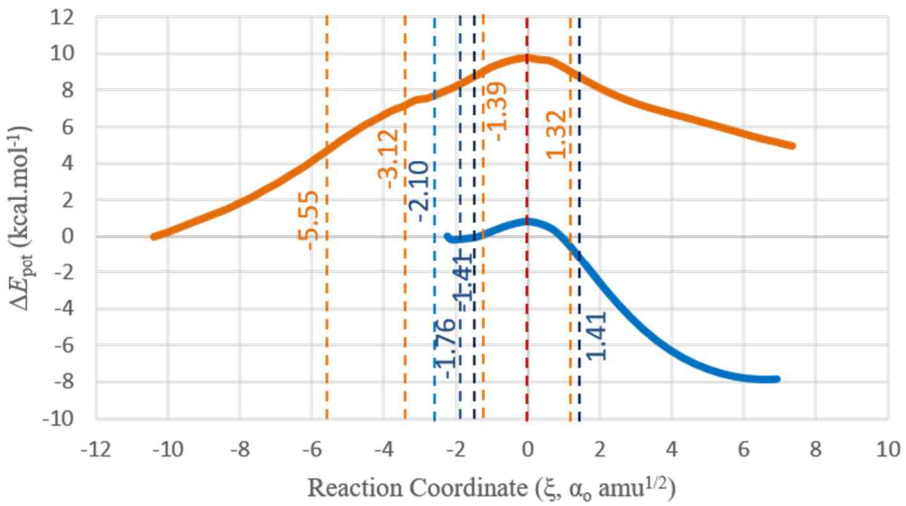

Figure 3. The energy profile for the reaction of Phenyl Carbonyl Isothiocyanate (Y=H) and Pyridine (X=H) in the gas-phase (—) and in the solvent model (—). The vertical dashed lines mark the reaction regions (ξ_i) calculated from the reaction force analysis.

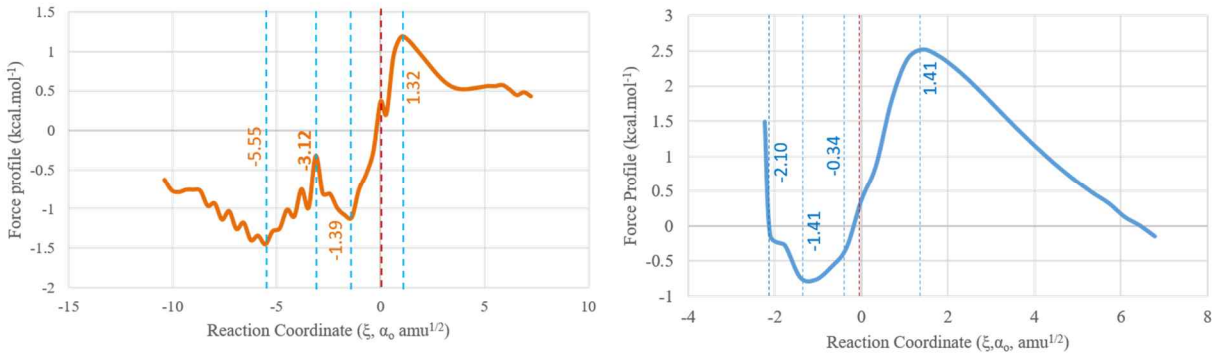

Figure 4. The reaction force profile for the substitution reaction between phenyl carbonyl isothiocyanate and pyridine in the gas (left) and in the solvent (right) model. The vertical dashed lines mark the reactant, intermediate, TS, Lg departure and the product regions.

These conclusions are in line with the unsubstituted reaction and corresponding energy profile, where the gas phase model is suggested to be endergonic, while the solvent phase is rather exergonic. However, an interestingly very small barrier energy in the solvent model of 1.23 kcal mol^{-1} (**Table 4**) was observed. The observation is probably due to the delocalization of the charge population stabilizing the associative type intermediate quite well by the solvation process.

Another interesting result is that the structural component (W_1) is large (56% concerning the activation energy) in the gas phase (**Table 4**). By contrast, the solvent model favorably regulates the reaction kinetically and thermodynamically.

In conclusion, it might be reasonable to state that the solvent takes full control over the structural and electronic components of the activation barrier, where spontaneous signs of progress have been seen for the polar solvent.

4.7 Reaction electronic flux

We estimated the reaction electronic flux (REF) for the intrinsic reaction coordinate using the chemical electronic potential following Eq. (11). The plots of calculated flux change for the gas phase and the solvent model throughout the reaction coordinate are displayed in **Figure 5**. The reactants were initially below the zero flux in the gas phase. As the reaction progressed, the relevant fluctuations of REF with a slightly elevated nature reflect the electronic transmission and the structural reorientation of both the nucleophile and the substrate towards the electrophilic center of the carbonyl moiety. The elevated flux indicates the adduct formation and the subsequent downward fall of REF for stabilization at the coordinate region ξ_1. The next step shows a slight elevation of REF with a great fluctuation, again indicating the intermediate formation as noted ξ_I in Eq. (7). After an insignificant stabilization process, while holding, the system was intended to move toward the TS in the region ξ_{TS} through the spontaneous region ξ_2. In this state, the magnitude of REF was sharply raised. The phenomena indicate the formation of the $C_1 - N_u$ bond. Then the magnitude of REF fell, accounting for the $C_1 - N_L$ bond breaking of –NCS Lg. This non-spontaneous electronic activity is located in the region of ξ_3 at the reaction coordinate. Finally, the reaction attended at the product state, PC.

We found a different nature of the REF for the solution model, inconsistent with the above phenomena. Sudden spontaneous electronic flux fluctuation is probably due to the solvent polarity assisted extended nucleophilic interaction during the short ξ_1 region in the coordinate. It forms an adduct in the region of ξ_I, where a $C_1 - N_u$ bond forming step is observed by elevation of the flux magnitude at the ξ_{TS}. A non-spontaneous flux then kinetically represents the $C_1 - N_L$ bond breaking. The solvent plays an important role, where it increases and modulates the electronic activity of the reaction and drastically shifts the flux peaks towards the reactant side.

By closely observing the ξ_{TS}, we may find only a positive flux associated with a single activity of density of the formation. This effect shifts to the left with increasing polarity. This formation is influenced by the solvent thermodynamically and kinetically as an existence of a lower barrier. Bond cleaving is kinetically conducted in the solvent model by solvation of the ion pairs. In turn, the solvent catalyzes the process towards the exoergic path. The Wiberg bond index crossing point of formation and breakage in the gas phase is closer before to the TS than in the solvent model (**SF5a**). Solvent polarity shifts the crossing point toward the left (reactant side, **SF5b**), indicating that more reactants like TS appear than in the gas phase. This observation is a clear manifestation of the Hammond postulate[103], where solvent-assisted TS stabilization was observed.

Contrary to the solvent model, the TS in the gas phase is more balanced, where the formation enhances bond breaking. Our findings agree with the observation from the Hammett treatment and the CIC point of view.

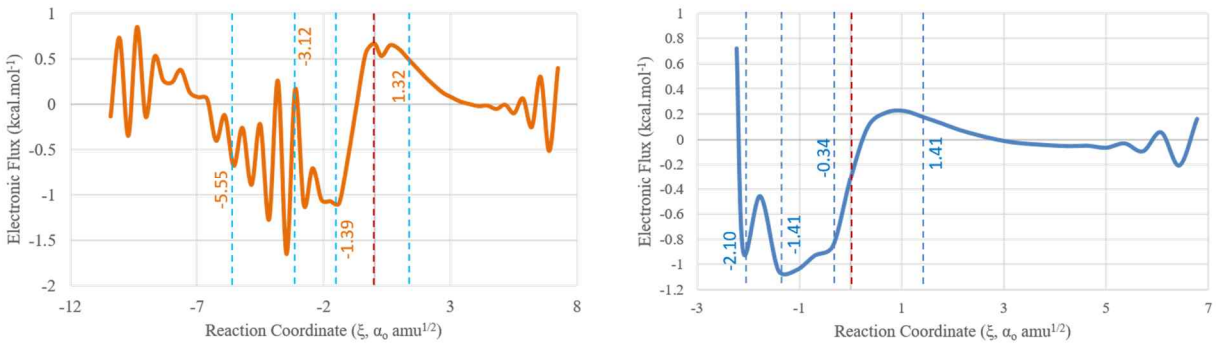

Figure 5. The reaction electronic flux profile for nucleophilic substitution reaction between pyridine and the phenyl carbonyl isothiocyanate in the gas phase (left) and in the solvent (right). The vertical line indicated the specific region of the interaction noted by the position (ξ_i) in the reaction coordinate.

Table 4. Corresponding reaction works (W_1 to W_6), activation energy ($\Delta E^{\ddagger}$) and reaction energy (ΔE_o) are displayed when phenyl carbonyl isothiocyanate and pyridine interacts each other in the gas phase and in the acetonitrile solvent. The qualitative property change can be observed. All energies shown are in kcal mol^{-1}.

Medium	W_1	W_2	W_3	W_4	W_5	W_6	$\Delta E^{\ddagger}$	ΔE_o	$\Delta E_o^{\ddagger}$	β
Gas	23.05	6.60	2.41	1.30	-1.20	-23.69	33.36	8.47	28.97	0.54
TS(g)			2.41	1.30	-1.20	-23.69	3.71	-21.18	11.96	0.59
Solvent	-0.02	0.10	0.80	0.04	-2.72	-36.94	0.91	-38.75	13.16	0.13
TS(s)			0.80	0.04	-2.72	-36.94	0.84	-38.82	12.97	0.13

4.8 The dual descriptor analysis

In the solution model, we found a different nature of the REF. An unexpected decrease for the flux fluctuation appears during the short ξ_1 region in the coordinate, due to the solvent assisted nucleophilic interaction. Subsequently, it forms an adduct in the region of ξ_I and a subsequent $C_1 - N_u$ bond forming step is observed by elevation of the flux magnitude at the ξ_{TS}. A non-spontaneous electronic flux then represents the $C_1 - N_L$ bond breaking. We found that the solvent plays an important role where it increases and modulates the electronic activity of the reaction and drastically shifts the flux peaks towards the reactant ride.

To project the local reactivity of the substitution process depending on the present reactants (XY = 33) in the gas phase are described sequentially for seven obtained steps, e.g., RC, ξ_1, I, ξ_2, TS, ξ_3, and PC, by analyzing the corresponding Fukui functions. The results are displayed in **Figure 6** (solvent model results are available, **SF8**). The electron density colors represent both the negatively charged (blue) lobes and the positively charged (green) lobes. The lobe size and the shape represent the density matrix and the orientations regarding the axis (not shown). The nucleophilic center has a moderately large electron density in the RC pyridine nitrogen. The C_1 reaction center in the substrate exists as an electrophilic center and the progress state ξ_1 changes with the expected degree of nucleophilicity. In the intermediate (I), nucleophiles already had formed a partial bond when O_2 and the O_3 dispersed the charge towards the phen-ring. In the TS, phen-ring enhances leaving group departure by pushing forward the negative charge. At this moment, the pyridine nucleophile achieved positive charge by forming azonium-type structure by increasing positive charge character. Finally, the reaction reaches the product state through ξ_3 to form PC, where Lg of the PC is developed as a nucleophilic character.

The actual nature of these state functions is nicely visible in the pictorial dual descriptor representation of the state density of ξ_1, I, TS, ξ_2, and ξ_3 from RC to the PC, see **Figure 6**. The presented results are in good agreement with the Pauling parameter analysis, energy analysis, NBO analysis, CIC results, and the reaction electronic flux. The solvent phase (**SF8**) reaction condenses electronic activity into the close states of the intermediate and the TS region with a strong nucleophilic interaction of early TS, where electronic activity behaves in a single step spontaneously.

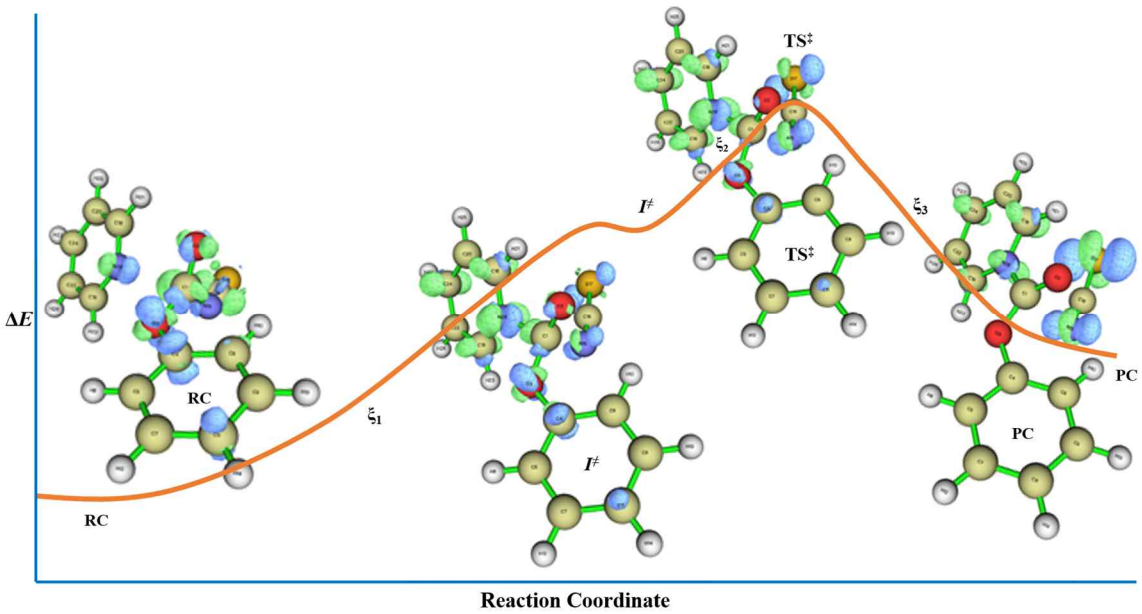

Figure 6. Dual descriptor densities for RC, ξ_1, I, ξ_2, TS, ξ_3, and PC for the studied substitution process in gas phase.

5. Conclusions

The interpretation of mechanism of the aminolysis reaction between Y-phenyl carbonyl isothiocyanates and X-pyridines has been computationally conducted in the gas phase and the continuum acetonitrile solvent polarization field at room temperature. In the present work, the

authors propose a stepwise mechanistic procedure for gas and continuum polarization field of acetonitrile models based on the following grounds:

(i) The pyridine nitrogen atom becomes considerably negatively charged in the TS in the solvent model based on extraordinarily large positive ρ_X and negative β_X values in the Hammett and Brönsted correlations (**Table 3**).

(ii) Strong bonding interaction occurs in the tetrahedral intermediate (**T**$^{\pm}$).

(iii) Partial positive charge development on the oxygen atom of the phenoxy ligand in the solvent model based on the –ve ρ_Y values (**Table 3**). However, +ve ρ_Y values are observed (**Table 2**) for the gas phase where azonium type N^+-residue may generate.

(iv) Strong bond (**Figure 5**) formation with a tight associative type intermediate for the gas and the solvent model showed large positive ρ_{XY} values (**Table 2**, **Table 3**).

(v) Reaction electronic flux indicated the existence of separate reaction regions throughout the reaction coordinate ξ, (**Figure 5**).

(vi) We found clear 3D potential paths (**Figure 7**) for the gas phase reactivity, where it can distinctively locate the position of the intermediate.

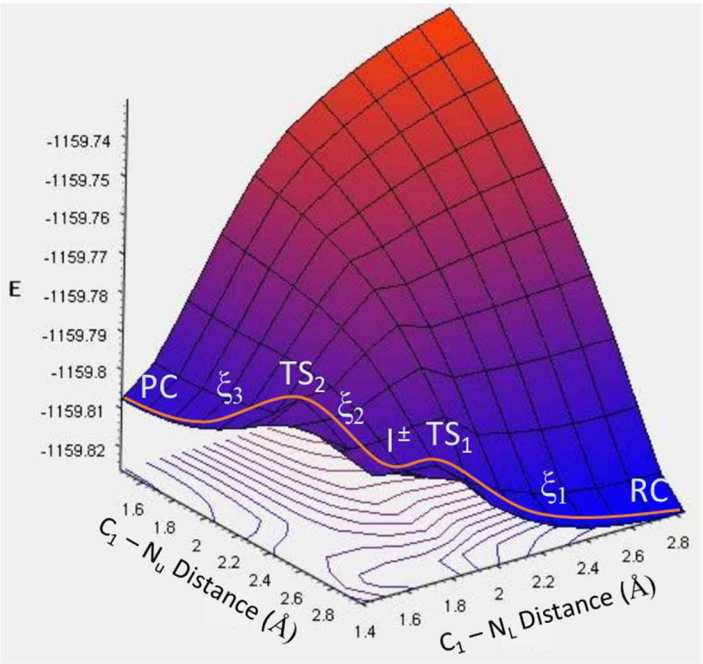

Figure 7. The 3D-potential path for the substitution reaction between pyridine and the phenyl carbonyl isothiocyanate in gas phase (Atomic distance in Å and energy, E, in hartree).

(vii) The dual density descriptor analysis confirms the above explanations (**Figure 6**) and fully agrees with the reported observations.

(viii) The investigated cross-interaction constants, ρ_{XY}, were large positive values (ρ_{XY} = 0.69 in the gas phase and 0.87 in the solvent model). They are strongly indicative of the stepwise mechanistic reaction criteria. The authors have considered a tetrahedral zwitterionic intermediate with stronger charge congestion in the gas phase followed by an H-bond interaction for the rate-limiting breakdown of the leaving group. However, a solvent-assisted non-spontaneous rate-limiting breakdown was observed in the polarization model with a relatively loose TS.

Acknowledgements

This work has been supported by the Research and Development Program of Ghent University Global Campus (GUGC), Korea. The authors thank Prof. Jonathan Ozelton from the Center for Language and Learning (LLC) at Ghent University Global Campus (GUGC) for proofreading of the document. The authors thank the Vlaams Supercomputer Centrum (VSC), funded by Ghent University.

Supplementary content

- Uploaded along submission.

References

(1) Kim, W. K.; Ryu, W. S.; Han, I.-S.; Kim, C. K.; Lee, I. Theoretical Studies on the Gas-Phase Nucleophilic Substitution Reactions of Benzyl Chlorides with Phenoxides and Thiophenoxides. *J. Phys. Org. Chem.* **1998**, *11* (2), 115–124. https://doi.org/10.1002/(SICI)1099-1395(199802)11:2<115::AID-POC985>3.0.CO;2-B.

(2) Wang Ki Kim; Wang Sun Ryu; Hyeong Yeoun Park; In-Suk Han; Chang Kon Kim; Ikchoon Lee. Theoretical Studies on the Nucleophilic Substitution Reactions of 1-Phenylethyl Chlorides. *Bull. Korean Chem. Soc. BKCS* **1997**, *18* (8), 868–873.

(3) Lee, I.; Kim, C. K.; Han, I. S.; Lee, H. W.; Kim, W. K.; Kim, Y. B. Theoretical Studies of Solvent Effect on the Basicity of Substituted Pyridines. *J. Phys. Chem. B* **1999**, *103* (34), 7302–7307. https://doi.org/10.1021/jp991115w.

(4) Kim, C. K.; Li, H. G.; Lee, B.-S.; Kim, C. K.; Lee, H. W.; Lee, I. Gas-Phase Identity Nucleophilic Substitution Reactions of Cyclopropenyl Halides. *J. Org. Chem.* **2002**, *67* (6), 1953–1960. https://doi.org/10.1021/jo0164047.

(5) Um, I.-H.; Chun, S.-M.; Chae, O.-M.; Fujio, M.; Tsuno, Y. Effect of Amine Nature on Reaction Rate and Mechanism in Nucleophilic Substitution Reactions of 2,4-Dinitrophenyl X-Substituted Benzenesulfonates with Alicyclic Secondary Amines. *J. Org. Chem.* **2004**, *69* (9), 3166–3172. https://doi.org/10.1021/jo049812u.

(6) Castro, E. A.; Ugarte, D.; Rojas, M. F.; Pavez, P.; Santos, J. G. Nucleophilic Substitution Reactions of Diethyl 4-Nitrophenyl Phosphate Triester: Kinetics and Mechanism. *Int. J. Chem. Kinet.* **2011**, *43* (12), 708–714. https://doi.org/10.1002/kin.20605.

(7) Aguayo, R.; Arias, F.; Cañete, A.; Zuñiga, C.; Castro, E. A.; Pavez, P.; Santos, J. G. Dual Nucleophilic Substitution Reactions of O,O-Diethyl 2,4-Dinitrophenyl Phosphate and

Thionophosphate Triesters. *Int. J. Chem. Kinet.* **2013**, *45* (3), 202–211. https://doi.org/10.1002/kin.20756.

(8) Lee, J.-P.; Bae, A.-R.; Im, L.-R.; Um, I.-H. A Kinetic Study on Aminolysis of 2-Pyridyl X-Substituted Benzoates: Effect of Changing Leaving Group from 4-Nitrophenolate to 2-Pyridinolate on Reactivity and Mechanism. *Bull. Korean Chem. Soc.* **2010**, *31* (12), 3588–3592. https://doi.org/10.5012/BKCS.2010.31.12.3588.

(9) Um, I.-H.; Im, L.-R.; Kim, E.-H.; Shin, J. H. Nonlinear Hammett Plots in Pyridinolysis of 2,4-Dinitrophenyl X-Substituted Benzoates: Change in RDS versus Resonance Contribution. *Org. Biomol. Chem.* **2010**, *8* (16), 3801–3806. https://doi.org/10.1039/C0OB00031K.

(10) Lee, H. W.; H.R. Barai; K.K. Adhikary. Kinetics and Mechanism of the Anilinolysis of Aryl Ethyl Isothiocyanophosphates in Acetonitrile. **2013**, *34* (6), 1829–1834. https://doi.org/10.5012/BKCS.2013.34.6.1829.

(11) Keshab Kumar Adhikary; Hai Whang Lee. Significant Substituent Effects on Pyridinolysis of Aryl Ethyl Chlorophosphates in Acetonitrile. *Bull Korean Chem Soc* **2014**, *35* (5), 1460–1464. https://doi.org/10.5012/bkcs.2014.35.5.1460.

(12) Ikchoon LEE1; Hai Whang LEE2. Cross-Interaction Constants. A Mechanistic Tool. *Collect Czech Chem Commun* **1999**, *64*, 1529–1550. https://doi.org/10.1135/cccc19991529.

(13) Herrera, B.; Toro-Labbé, A. The Role of Reaction Force and Chemical Potential in Characterizing the Mechanism of Double Proton Transfer in the Adenine−Uracil Complex. *J. Phys. Chem. A* **2007**, *111* (26), 5921–5926. https://doi.org/10.1021/jp065951z.

(14) Cerón, M. L.; Echegaray, E.; Gutiérrez-Oliva, S.; Herrera, B.; Toro-Labbé, A. The Reaction Electronic Flux in Chemical Reactions. *Sci. China Chem.* **2011**, *54* (12), 1982–1988. https://doi.org/10.1007/s11426-011-4447-z.

(15) Duarte, F.; Toro-Labbé, A. The Catalytic Effect of Water on the Keto-Enol Tautomerisation Reaction of Thioformic Acid. *Mol. Phys.* **2010**, *108* (10), 1375–1384. https://doi.org/10.1080/00268971003698064.

(16) Litow, B. On Hadamard Square Roots of Unity. *Theor. Comput. Sci.* **2000**, *237* (1), 447–454. https://doi.org/10.1016/S0304-3975(99)00327-8.

(17) Gresser, M. J.; Jencks, W. P. Ester Aminolysis. Structure-Reactivity Relationships and the Rate-Determining Step in the Aminolysis of Substituted Diphenyl Carbonates. *J. Am. Chem. Soc.* **1977**, *99* (21), 6963–6970. https://doi.org/10.1021/ja00463a032.

(18) Gresser, M. J.; Jencks, W. P. Ester Aminolysis. Partitioning of the Tetrahedral Addition Intermediate, T.+-., and the Relative Leaving Ability of Nitrogen and Oxygen. *J. Am. Chem. Soc.* **1977**, *99* (21), 6970–6980. https://doi.org/10.1021/ja00463a033.

(19) Castro, E. A.; Santander, C. L. Nonlinear Broensted-Type Plot in the Pyridinolysis of 2,4-Dinitrophenyl Benzoate in Aqueous Ethanol. *J. Org. Chem.* **1985**, *50* (19), 3595–3600. https://doi.org/10.1021/jo00219a029.

(20) Oh, H. K.; Shin, C. H.; Lee, I. Kinetics and Mechanism of the Aminolysis of Phenyl Dithiobenzoates. *J. Chem. Soc. Perkin Trans. 2* **1995**, No. 6, 1169–1173. https://doi.org/10.1039/P29950001169.

(21) Kim, T.-H.; Huh, C.; Lee, B.-S.; Lee, I. Nucleophilic Substitution Reactions of Cinnamoyl Chlorides with Anilines in Acetonitrile and Acetonitrile–Methanol Mixtures.

J. Chem. Soc. Perkin Trans. 2 **1995**, No. 12, 2257–2261. https://doi.org/10.1039/P29950002257.

(22) Toro-Labbé, A. Characterization of Chemical Reactions from the Profiles of Energy, Chemical Potential, and Hardness. *J. Phys. Chem. A* **1999**, *103* (22), 4398–4403. https://doi.org/10.1021/jp984187g.

(23) Gutiérrez-Oliva, S.; Herrera, B.; Toro-Labbé, A.; Chermette, H. On the Mechanism of Hydrogen Transfer in the HSCH(O) ⇌ (S)CHOH and HSNO ⇌ SNOH Reactions. *J. Phys. Chem. A* **2005**, *109* (8), 1748–1751. https://doi.org/10.1021/jp0452756.

(24) Herrera, B.; Toro-Labbe, A. The Role of the Reaction Force to Characterize Local Specific Interactions That Activate the Intramolecular Proton Transfers in DNA Basis. *J. Chem. Phys.* **2004**, *121* (15), 7096–7102. https://doi.org/10.1063/1.1792091.

(25) Marcus, R. A. Chemical and Electrochemical Electron-Transfer Theory. *Annu. Rev. Phys. Chem.* **1964**, *15* (1), 155–196. https://doi.org/10.1146/annurev.pc.15.100164.001103.

(26) Leffler, J. E. Parameters for the Description of Transition States. *Science* **1953**, *117* (3039), 340–341. https://doi.org/10.1126/science.117.3039.340.

(27) Reed, A. E.; Curtiss, L. A.; Weinhold, F. Intermolecular Interactions from a Natural Bond Orbital, Donor-Acceptor Viewpoint. *Chem. Rev.* **1988**, *88* (6), 899–926. https://doi.org/10.1021/cr00088a005.

(28) Morell, C.; Grand, A.; Toro-Labbé, A. New Dual Descriptor for Chemical Reactivity. *J. Phys. Chem. A* **2005**, *109* (1), 205–212. https://doi.org/10.1021/jp046577a.

(29) Morell, C.; Grand, A.; Toro-Labbé, A. Theoretical Support for Using the Δf(r) Descriptor. *Chem. Phys. Lett.* **2006**, *425* (4), 342–346. https://doi.org/10.1016/j.cplett.2006.05.003.

(30) Ayers, P. W.; Morell, C.; De Proft, F.; Geerlings, P. Understanding the Woodward–Hoffmann Rules by Using Changes in Electron Density. *Chem. – Eur. J.* **2007**, *13* (29), 8240–8247. https://doi.org/10.1002/chem.200700365.

(31) Fukui, K. Formulation of the Reaction Coordinate. *J. Phys. Chem.* **1970**, *74* (23), 4161–4163. https://doi.org/10.1021/j100717a029.

(32) Fukui, K. The Path of Chemical Reactions - the IRC Approach. *Acc. Chem. Res.* **1981**, *14* (12), 363–368. https://doi.org/10.1021/ar00072a001.

(33) Gonzalez, C.; Schlegel, H. B. An Improved Algorithm for Reaction Path Following. *J. Chem. Phys.* **1989**, *90* (4), 2154–2161. https://doi.org/10.1063/1.456010.

(34) Hratchian, H. P.; Schlegel, H. B. Accurate Reaction Paths Using a Hessian Based Predictor–Corrector Integrator. *J. Chem. Phys.* **2004**, *120* (21), 9918–9924. https://doi.org/10.1063/1.1724823.

(35) Hratchian, H. P.; Schlegel, H. B. Using Hessian Updating To Increase the Efficiency of a Hessian Based Predictor-Corrector Reaction Path Following Method. *J. Chem. Theory Comput.* **2005**, *1* (1), 61–69. https://doi.org/10.1021/ct0499783.

(36) Toro-Labbé, A.; Gutiérrez-Oliva, S.; Murray, J. S.; Politzer, P. The Reaction Force and the Transition Region of a Reaction. *J. Mol. Model.* **2009**, *15* (6), 707–710. https://doi.org/10.1007/s00894-008-0431-8.

(37) Politzer, P.; Toro-Labbé, A.; Gutiérrez-Oliva, S.; Herrera, B.; Jaque, P.; Concha, M. C.; Murray, J. S. The Reaction Force: Three Key Points along an Intrinsic Reaction Coordinate. *J. Chem. Sci.* **2005**, *117* (5), 467–472. https://doi.org/10.1007/BF02708350.

(38) Echegaray, E.; Toro-Labbé, A. Reaction Electronic Flux: A New Concept To Get Insights into Reaction Mechanisms. Study of Model Symmetric Nucleophilic Substitutions. *J. Phys. Chem. A* **2008**, *112* (46), 11801–11807. https://doi.org/10.1021/jp805225e.

(39) Vogt-Geisse, S.; Toro-Labbé, A. The Mechanism of the Interstellar Isomerization Reaction HOC+→HCO+ Catalyzed by H2: New Insights from the Reaction Electronic Flux. *J. Chem. Phys.* **2009**, *130* (24), 244308. https://doi.org/10.1063/1.3147702.

(40) Rincón, E.; Jaque, P.; Toro-Labbé, A. Reaction Force Analysis of the Effect of Mg(II) on the 1,3 Intramolecular Hydrogen Transfer in Thymine. *J. Phys. Chem. A* **2006**, *110* (30), 9478–9485. https://doi.org/10.1021/jp062870u.

(41) Politzer, P.; Burda, J. V.; Concha, M. C.; Lane, P.; Murray, J. S. Analysis of the Reaction Force for a Gas Phase SN2 Process: CH3Cl + H2O CH3OH + HCl*J. Phys. Chem. A* **2006**, *110* (2), 756–761. https://doi.org/10.1021/jp0582080.

(42) Calais, J.-L. Density-Functional Theory of Atoms and Molecules. R.G. Parr and W. Yang, Oxford University Press, New York, Oxford, 1989. IX + 333 Pp. Price £45.00. *Int. J. Quantum Chem.* **1993**, *47* (1), 101–101. https://doi.org/10.1002/qua.560470107.

(43) Geerlings, P.; De Proft, F.; Langenaeker, W. Conceptual Density Functional Theory. *Chem. Rev.* **2003**, *103* (5), 1793–1874. https://doi.org/10.1021/cr990029p.

(44) Anderson, J. S. M.; Melin, J.; Ayers, P. W. Conceptual Density-Functional Theory for General Chemical Reactions, Including Those That Are Neither Charge- nor Frontier-

Orbital-Controlled. 1. Theory and Derivation of a General-Purpose Reactivity Indicator. *J. Chem. Theory Comput.* **2007**, *3* (2), 358–374. https://doi.org/10.1021/ct600164j.

(45) Wu, Q.; Ayers, P. W.; Yang, W. Density-Functional Theory Calculations with Correct Long-Range Potentials. *J. Chem. Phys.* **2003**, *119* (6), 2978–2990. https://doi.org/10.1063/1.1590631.

(46) Ayers, P. W.; Parr, R. G.; Pearson, R. G. Elucidating the Hard/Soft Acid/Base Principle: A Perspective Based on Half-Reactions. *J. Chem. Phys.* **2006**, *124* (19), 194107. https://doi.org/10.1063/1.2196882.

(47) Bartolotti, L. J.; Ayers, P. W. An Example Where Orbital Relaxation Is an Important Contribution to the Fukui Function. *J. Phys. Chem. A* **2005**, *109* (6), 1146–1151. https://doi.org/10.1021/jp0462207.

(48) Koopmans, T. Über Die Zuordnung von Wellenfunktionen Und Eigenwerten Zu Den Einzelnen Elektronen Eines Atoms. *Physica* **1934**, *1* (1), 104–113. https://doi.org/10.1016/S0031-8914(34)90011-2.

(49) Sandeep, K.; Siva Reddy, A.; Kumara Swamy, K. C. Cu(i) Catalysed Annulation of Isothiocyanates/Isocyanates with 2-Iodo-Sulfonamides: Synthesis of Benzodithiazines, Benzothiadiazinones, Benzothiazinylidene-Anilines and Benzothiazolylidene-Anilines. *Org. Biomol. Chem.* **2019**, *17* (28), 6880–6894. https://doi.org/10.1039/C9OB00994A.

(50) Gupta P, Wright SE, Kim SH, Srivastava SK. Phenethyl Isothiocyanate: A Comprehensive Review of Anti-Cancer Mechanisms. *Biochim Biophys Acta* **2014**, *1846* (2), 405-24. https://doi.org/doi: 10.1016/j.bbcan.2014.08.003. Epub 2014 Aug 23. PMID: 25152445; PMCID: PMC4260992.

(51) Kim YJ; Lee DH; Ahn J; Chung WJ; Jang YJ; Seong KS; Moon JH; Ha TY; Jung CH. Pharmacokinetics, Tissue Distribution, and Anti-Lipogenic/Adipogenic Effects of Allyl-Isothiocyanate Metabolites. *PLoS One* **2015**, *28* (10(8)), e0132151. https://doi.org/doi: 10.1371/journal.pone.0132151.

(52) Massarotti, A.; Brunelli, F.; Aprile, S.; Giustiniano, M.; Tron, G. C. Medicinal Chemistry of Isocyanides. *Chem. Rev.* **2021**, *121* (17), 10742–10788. https://doi.org/10.1021/acs.chemrev.1c00143.

(53) Lee, K. S.; Adhikary, K. K.; Lee, H. W.; Lee, B.-S.; Lee, I. Nucleophilic Substitution Reactions of α-Chloroacetanilides with Benzylamines in Dimethyl Sulfoxide. *Org. Biomol. Chem.* **2003**, *1* (11), 1989–1994. https://doi.org/10.1039/B300477E.

(54) Shuchismita Dey; Keshab Kumar Adhikary; Chan Kyung Kim; Bon-Su Lee; Hai Whang Lee. Nucleophilic Substitution Reactions of α-Chloroacetanilides with Pyridines in Dimethyl Sulfoxide. *Bull Korean Chem Soc* **2005**, *26* (5), 776–780. https://doi.org/10.5012/bkcs.2005.26.5.776.

(55) Keshab Kumar Adhikary; Chan Kyung Kim; Bon-Su Lee; Hai Whang Lee. Nucleophilic Substitution Reactions of α-Bromoacetanilides with Benzylamines. *Bull Korean Chem Soc* **2008**, *29* (1), 191–196. https://doi.org/10.5012/bkcs.2008.29.1.191.

(56) Keshab Kumar Adhikary; Hai Whang Lee. Nucleophilic Substitution Reactions of N-Methyl α-Bromoacetanilides with Benzylamines in Dimethyl Sulfoxide. *Bull Korean Chem Soc* **2011**, *32* (3), 857–862. https://doi.org/10.5012/bkcs.2011.32.3.857.

(57) Oh, H. K.; Ku, M. H.; Lee, H. W.; Lee, I. Kinetics and Mechanism of the Pyridinolysis of Aryl Furan-2-Carbodithioates in Acetonitrile. *J. Org. Chem.* **2002**, *67* (25), 8995–8998. https://doi.org/10.1021/jo0264269.

(58) Oh, H. K.; Ku, M. H.; Lee, H. W.; Lee, I. Nucleophilic Substitution Reactions of Aryl Dithioacetates with Pyridines in Acetonitrile. *J. Org. Chem.* **2002**, *67* (11), 3874–3877. https://doi.org/10.1021/jo025637a.

(59) Dyson, P. J.; Jessop, P. G. Solvent Effects in Catalysis: Rational Improvements of Catalysts via Manipulation of Solvent Interactions. *Catal. Sci. Technol.* **2016**, *6* (10), 3302–3316. https://doi.org/10.1039/C5CY02197A.

(60) Adhikary, K. K.; Lee, H.-W.; Lee, I.-C. Kinetics and Mechanism of the Pyridinolysis of Aryl Phenyl Isothiocyanophosphate in Acetonitrile. *Bull. Korean Chem. Soc.* **2003**, *24* (8), 1135–1140. https://doi.org/10.5012/bkcs.2003.24.8.1135.

(61) Keshab Kumar Adhikary; Hai Whang Lee. Kinetics and Mechanism of the Pyridinolysis of Dimethyl Isothiocyanophosphate in Acetonitrile. *Bull Korean Chem Soc* **2012**, *33* (7), 2260–2264. https://doi.org/10.5012/bkcs.2012.33.7.2260.

(62) Keshab Kumar Adhikary; Hai Whang Lee. Kinetics and Mechanism of the Pyridinolysis of Diethyl Isothiocyanophosphate in Acetonitrile. *Bull Korean Chem Soc* **2012**, *33* (3), 1042–1046. https://doi.org/10.5012/bkcs.2012.33.3.1042.

(63) Hasi Rani Barai; Keshab Kumar Adhikary; Hai Whang Lee. Anilinolysis of Dimethyl Isothiocyanophosphate in Acetonitrile. *Bull Korean Chem Soc* **2012**, *33* (8), 2769–2772. https://doi.org/10.5012/bkcs.2012.33.8.2769.

(64) Hasi Rani Barai; Keshab Kumar Adhikary; Hai Whang Lee. Anilinolysis of Diethyl Isothiocyanophosphate in Acetonitrile. *Bull. Korean Chem. Soc.* **2012**, *33* (3), 1089–1092. https://doi.org/10.5012/bkcs.2012.33.3.1089.

(65) Vennelakanti, V.; Nazemi, A.; Mehmood, R.; Steeves, A. H.; Kulik, H. J. Harder, Better, Faster, Stronger: Large-Scale QM and QM/MM for Predictive Modeling in Enzymes and

Proteins. *Curr. Opin. Struct. Biol.* **2022**, *72*, 9–17. https://doi.org/10.1016/j.sbi.2021.07.004.

(66) Guha, R.; Willighagen, E. A Survey of Quantitative Descriptions of Molecular Structure. *Curr. Top. Med. Chem.* **2012**, *12* (18), 1946–1956. https://doi.org/10.2174/156802612804910278.

(67) Savin, A.; Becke, A. D.; Flad, J.; Nesper, R.; Preuss, H.; von Schnering, H. G. A New Look at Electron Localization. *Angew. Chem. Int. Ed. Engl.* **1991**, *30* (4), 409–412. https://doi.org/10.1002/anie.199104091.

(68) Menger, F. M.; Glass, L. E. Dominance of an Ionic Mechanism over a Cyclic Concerted Process in a Hydrocabon Solvent. *J. Org. Chem.* **1974**, *39* (16), 2469–2470. https://doi.org/10.1021/jo00930a052.

(69) Shawali, A. S.; Harhash, A.; Sidky, M. M.; Hassaneen, H. M.; Elkaabi, S. S. Kinetics and Mechanism of Aminolysis of Carbamates. *J. Org. Chem.* **1986**, *51* (18), 3498–3501. https://doi.org/10.1021/jo00368a020.

(70) Koh, H. J.; Kim, O. S.; Lee, H. W.; Lee, I. Kinetics and Mechanism of the Aminolysis of P-Nitrophenyl N-Phenylcarbamates. *J. Phys. Org. Chem.* **1997**, *10* (10), 725–730. https://doi.org/10.1002/(SICI)1099-1395(199710)10:10<725::AID-POC943>3.0.CO;2-X.

(71) Oh, H. K.; Park, J. E.; Sung, D. D.; Lee, I. Nucleophilic Substitution Reactions of Aryl N-Phenyl Thiocarbamates with Benzylamines in Acetonitrile. *J. Org. Chem.* **2004**, *69* (9), 3150–3153. https://doi.org/10.1021/jo049845+.

(72) Oh, H. K.; Jin, Y. C.; Sung, D. D.; Lee, I. Kinetics and Mechanism of the Aminolysis of Aryl Thiocarbamates: Effects of the Non-Leaving Group. *Org. Biomol. Chem.* **2005**, *3* (7), 1240–1244. https://doi.org/10.1039/B500251F.

(73) Castro, E. A.; Cubillos, M.; Iglesias, R.; Santos, J. G. Concerted Aminolysis of Diaryl Carbonates: Kinetic Sensitivity on the Basicity of the Nucleophile, Nonleaving Group, and Nucleofuge. *Int. J. Chem. Kinet.* **2012**, *44* (9), 604–611. https://doi.org/10.1002/kin.20700.

(74) Sung, K.; Zhuang, B.-R.; Huang, P.-M.; Jhong, S.-W. Kinetic and Mechanistic Studies of NEt_3-Catalyzed Intramolecular Aminolysis of Carbamate. *J. Org. Chem.* **2008**, *73* (11), 4027–4033. https://doi.org/10.1021/jo800306r.

(75) Hanna Lee; Hyuck Keun Oh. Kinetics and Mechanism of the Aminolysis of Aryl N-Allyl Thiocarbamates in Acetonitrile. *Bull Korean Chem Soc* **2010**, *31* (2), 475–478. https://doi.org/10.5012/bkcs.2010.31.2.475.

(76) Liu, C.; Chen, Y.; Sun, Y.; Wu, F. Crystal Structure and Mechanistic Investigation of the Reaction of 5-Amino-1-(2,6-Dichloro-4-(Trifluoromethyl)Phenyl)-1H-Pyrazole-3-Carbonitrile with Unsaturated Carbonyl Compounds. *Res. Chem. Intermed.* **2013**, *39* (5), 2087–2093. https://doi.org/10.1007/s11164-012-0740-5.

(77) Eagon, S.; DeLieto, C.; McDonald, W. J.; Haddenham, D.; Saavedra, J.; Kim, J.; Singaram, B. Mild and Expedient Asymmetric Reductions of α,β-Unsaturated Alkenyl and Alkynyl Ketones by TarB-NO_2 and Mechanistic Investigations of Ketone Reduction. *J. Org. Chem.* **2010**, *75* (22), 7717–7725. https://doi.org/10.1021/jo101530f.

(78) Prasad, N.; Mohana, K. N. Mechanistic Investigation of Oxidation of Phenylpropanolamine with N-Bromobenzenesulfonamide in Alkaline Medium: A Kinetic Approach. *E-J. Chem.* **1900**, *5*, 348482. https://doi.org/10.1155/2008/348482.

(79) Pliego, Jr., Josefredo R.; Riveros, J. M. The Gas-Phase Reaction between Hydroxide Ion and Methyl Formate: A Theoretical Analysis of the Energy Surface and Product Distribution. *Chem. – Eur. J.* **2001**, *7* (1), 169–175. https://doi.org/10.1002/1521-3765(20010105)7:1<169::AID-CHEM169>3.0.CO;2-E.

(80) Mielby, J.; Riisager, A.; Fristrup, P.; Kegnæs, S. Mechanistic Investigation of the One-Pot Formation of Amides by Oxidative Coupling of Alcohols with Amines in Methanol. *Catal. Today10th Eur. Workshop Meet. Sel. Oxid. Silver Jubil. Meet. Sel. Key Sustain.* **2013**, *203*, 211–216. https://doi.org/10.1016/j.cattod.2012.04.026.

(81) Michlik, S.; Kempe, R. A Sustainable Catalytic Pyrrole Synthesis. *Nat. Chem.* **2013**, *5* (2), 140–144. https://doi.org/10.1038/nchem.1547.

(82) Gonzalez, Carlos.; Schlegel, H. Bernhard. Reaction Path Following in Mass-Weighted Internal Coordinates. *J. Phys. Chem.* **1990**, *94* (14), 5523–5527. https://doi.org/10.1021/j100377a021.

(83) Becke, A. D. Density-functional Thermochemistry. The Role of Exact Exchange. *J. Chem. Phys.* **1993**, *98* (7), 5648–5652. https://doi.org/10.1063/1.464913.

(84) W.J. Hehre; L. Radom; P.V.R. Schleyer; J.A. Pople. *Ab Initio Molecular Orbital Theory*; Wiley: New York, 1986.

(85) Tian Lu; Feiwu Chen. Multiwfn: A Multifunctional Wavefunction Analyzer. *J Comput Chem* **2012**, *33*, 580–592.

(86) Kubelka, J.; Bickelhaupt, F. M. Activation Strain Analysis of S_N2 Reactions at C, N, O, and F Centers. *J. Phys. Chem. A* **2017**, *121* (4), 885–891. https://doi.org/10.1021/acs.jpca.6b12240.

(87) F. D. Hardcastle. Valence-Length Correlations for Chemical Bonds from Atomic Orbital Exponents. *J. Ark. Acad. Sci.* **2013**, *67* (11), 53–58.

(88) F. D. Hardcastle. A General Valence-Length Correlation for Determining Bond Orders: Application to Carbon-Carbon and Carbon-Hydrogen Chemical Bonds. *J. Ark. Acad. Sci.* **2016**, *Vol. 70, Article 17.* (Article 17), 96–101.

(89) Hansch, Corwin.; Leo, A.; Taft, R. W. A Survey of Hammett Substituent Constants and Resonance and Field Parameters. *Chem. Rev.* **1991**, *91* (2), 165–195. https://doi.org/10.1021/cr00002a004.

(90) Coetzee, J. F. Ionic Reactions in Acetonitrile. In *Progress in Physical Organic Chemistry*; John Wiley & Sons, Ltd, 2007; pp 45–92. https://doi.org/10.1002/9780470171837.ch2.

(91) Spillane, W. J.; Hogan, G.; McGrath, P.; King, J.; Brack, C. Aminolysis of Sulfamate Esters in Non-Aqueous Solvents. Evidence Consistent with a Concerted E2-Type Mechanism. *J. Chem. Soc. Perkin Trans. 2* **1996**, No. 10, 2099–2104. https://doi.org/10.1039/P29960002099.

(92) NASER FOROUGHIF; R,' KENNETH T. LEFFE; YONG GU LEE. Basicity of Substituted 2-Pyridyl-1,1,3,3-Tetramethylguanidines and Aminopyridines in Acetonitrile and Water Solvents. *Can. J. Chem.* **1992**, *70*, 2856–2858.

(93) C.D. Ritchie. *Solution-Solvent Interactions*; Marcel-Dakker: New York, 1969.

(94) Foroughifar, N.; Leffek, K. T.; Lee, Y. G. Basicity of Substituted 2-Pyridyl-1,1,3,3-Tetramethylguanidines and Aminopyridines in Acetonitrile and Water Solvents. *Can. J. Chem.* **1992**, *70* (12), 2856–2858. https://doi.org/10.1139/v92-363.

(95) Albert, A.; Serjeant, E.P. *The Determination of Ionization Constants, 3rd Ed.*; Chapman and Hall: New York, 1984.

(96) Dean, J.A. *Handbook of Organic Chemistry*; McGraw-Hill: New York, 1987.

(97) Fischer, A.; Galloway, W. J.; Vaughan, J. Structure and Reactivity in the Pyridine Series. Part I. Acid Dissociation Constants of Pyridinium Ions. *J. Chem. Soc. Resumed* **1964**, No. 0, 3591–3596. https://doi.org/10.1039/JR9640003591.

(98) Koh, H. J.; Han, K. L.; Lee, H. W.; Lee, I. Kinetics and Mechanism of the Pyridinolysis of Phenyl Chloroformates in Acetonitrile. *J. Org. Chem.* **1998**, *63* (26), 9834–9839. https://doi.org/10.1021/jo9814905.

(99) Dixon, D. A.; Charlier, P. A.; Gassman, P. G. Mesomeric Stabilization of Carbonium Ions by .Alpha.-Cyano Groups. A Theoretical Evaluation of Inductive vs. Resonance Effects of the Cyano Moiety. *J. Am. Chem. Soc.* **1980**, *102* (11), 3957–3959. https://doi.org/10.1021/ja00531a051.

(100) Paddon-Row, M. N.; Santiago, C.; Houk, K. N. Possibility of .Pi.-Electron Donation by the Electron-Withdrawing Substituents CN, CHO, CF_3, and $^{+}NH_3$. *J. Am. Chem. Soc.* **1980**, *102* (21), 6561–6563. https://doi.org/10.1021/ja00541a033.

(101) Olah, G. A.; Arvanaghi, M.; Prakash, G. K. S. Stable Carbocations. Preparation and Carbon-13 and Nitrogen-15 NMR Spectroscopic Study of Cyanocarbenium Ions. Substituent Effects on the Extent of Mesomeric Nitrenium Ion Character in

Cyanodiphenylmethyl Cations. The Search for Related Stable .Alpha.-Cyanocarbenium Ions. *J. Am. Chem. Soc.* **1982**, *104* (6), 1628–1631. https://doi.org/10.1021/ja00370a030.

(102) Krishnamurthy, V. V.; Prakash, G. K. Surya.; Iyer, P. S.; Olah, G. A. Stable Carbocations. Study of Carbon-13-Carbon-13 NMR Coupling Constants in .Alpha.-Cyanodiarylmethyl and 1,1-Diaryl-2-Butynyl Cations. *J. Am. Chem. Soc.* **1986**, *108* (7), 1575–1579. https://doi.org/10.1021/ja00267a029.

(103) Hammond, G. S. A Correlation of Reaction Rates. *J. Am. Chem. Soc.* **1955**, *77* (2), 334–338. https://doi.org/10.1021/ja01607a027.

(104) Solà, M.; Toro-Labbé, A. The Hammond Postulate and the Principle of Maximum Hardness in Some Intramolecular Rearrangement Reactions. *J. Phys. Chem. A* **1999**, *103* (44), 8847–8852. https://doi.org/10.1021/jp990576e.